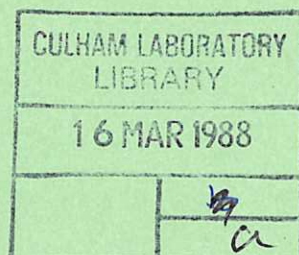# ECRH current drive studies in the CLEO tokamak

B. Lloyd
M. O'Brien
M. W. Alcock
M. Cox
A. C. Riviere
A. Simonetto
T. N. Todd

T. Edlington
N. R. Ainsworth
P. R. Collins
A. N. Dellis
D. C. Robinson
D. F. H. Start

UK ATOMIC ENERGY AUTHORITY

Culham Laboratory

ECRH current drive studies in the CLEO tokamak

B. Lloyd   T. Edlington   M. O'Brien
N. R. Ainsworth   M. W. Alcock   P. R. Collins
M. Cox   A. N. Dellis   A. C. Riviere
D. C. Robinson   A. Simonetto   D. F. H. Start
T. N. Todd

Culham Laboratory, Abingdon, Oxon OX14 3DB

(UKAEA/Euratom Fusion Association)

ABSTRACT

Non-inductive current drive using second harmonic ECRH at both 28 GHz and 60 GHz has been studied in the CLEO tokamak. At 60 GHz RF driven currents of up to 5 kA have been observed at $\bar{n}_e$ = 4 x 10^{18} m^{-3} for 185 kW of injected power indicating an efficiency of $\eta \equiv \bar{n}_e I_{rf} R_0 / P_{rf}$ = 0.001 (10^{20} m^{-3} AmW^{-1}). The RF driven current scaled linearly with total plasma current in the range 5-15 kA and was maximised when the cyclotron resonance was located near to the centre of the plasma. Sawtooth activity was normally strongly affected and transient sawtooth stabilisation was often observed. Detailed theoretical studies are able to reproduce both the high absorption efficiencies and the scaling of RF driven current with resonance position seen in the 60 GHz experiments. However the magnitude of the observed current is a factor of ~ 3 below that theoretically predicted. At 28 GHz no evidence of RF driven currents could be detected. Possible reasons for this are discussed.

1. INTRODUCTION

The study of non-inductive current drive using electromagnetic waves
has received much attention in recent years. Most experimental effort
has been devoted to the use of the lower hybrid slow wave and this
particular scheme is now well-established both experimentally [1] and
theoretically [2-5]. However the extrapolation of lower hybrid current
drive (LHCD) to the reactor regime is not straight-forward [6]. Due to
the effects of accessibility, strong electron Landau damping and the
need to avoid interaction with the fusion generated alpha particles one
is restricted to current drive in the outer regions of the plasma which
may lead to the development of unstable profiles. Other RF current
drive schemes have been suggested theoretically. In particular, Fisch
and Boozer [7] have pointed out that preferential heating of electrons
moving in a particular direction to the magnetic field leads to the
development of an RF driven plasma current via the creation of an
asymmetric resistivity. This mechanism lies at the heart of the LHCD
scheme but more importantly allows for the possibility of RF current
drive using electron cyclotron waves, which induce velocity space
diffusion primarily in the perpendicular direction. As in the case of
LHCD, the launched waves must be directed with a finite net $k_\parallel$
(wavenumber parallel to the magnetic field). However, contrary to
earlier assumptions, Cairns et al [8] have shown that strong absorption
of the waves in a single pass through the plasma is not necessary in

order to drive a non-zero total current. This conclusion is reached
from consideration of the effect on the electron cyclotron resonance
condition of the relativistic correction arising from the velocity
dependence of the electron cyclotron frequency. The most important
result of this correction is that the current driven in the plasma in
response to a given wave amplitude is, in an inhomogeneous field, no
longer antisymmetric about the cyclotron resonance layer. This effect
is important even at a temperature of 1 keV.

The first observations of plasma currents driven by waves at the
electron cyclotron resonance were made in the Culham Superconducting
Levitron [9]. The current was observed to flow in opposite directions
on opposite sides of the cyclotron layer and was found to scale
linearly with microwave power and with T_e/n_e in accordance with theory.
Subsequently RF current drive at the second electron cyclotron harmonic
was demonstrated in the TOSCA tokamak [10] where the strong reduction
in current drive efficiency observed when the resonance was located at
large major radius $(R>R_0)$ was attributed to the influence of electron
trapping. More recently electron cyclotron current drive has been
studied at the fundamental and second harmonic in WT-2 [11] and WT-3
[12] respectively, where in each case the total plasma current could be
supported by the waves. However in both experiments the direction of
the wave-driven current was independent of the direction of wave
propagation and the mechanism of current drive was attributed to the

interaction of the waves with a pre-existing superthermal tail in the ohmically heated slideaway target plasma.

Here we report the results of a systematic study of second harmonic electron cyclotron current drive in the CLEO tokamak at both 28 GHz and 60 GHz in hot ($\gtrsim$ 1 keV) well-controlled plasmas using well-defined launched wave spectra. The techniques used to inject the waves into the plasma are outlined in section 2 together with the salient features of the tokamak design. In sections 3 and 4 the results of experiments at 60 GHz and 28 GHz respectively are described. A combined Fokker-Planck and ray tracing code has been used to study the expected wave-plasma interaction and the theoretical predictions are presented and compared with the experimental results in section 5. Finally, a summary and discussion of the results is given in section 6.

2. TECHNICAL DETAILS

The CLEO device has been described in detail elsewhere [13]. Although the present version was originally designed as an ℓ = 3 stellarator, in recent years it has operated primarily as an iron-core tokamak of major radius R_o = 0.9m and minor radius a = 0.13m as defined by two poloidal tungsten limiters placed 180° apart toroidally. Feedback control of plasma current, line-averaged electron density and both vertical and horizontal plasma position allow well-controlled reproducible plasmas to be established with pulse durations up to 0.5s. Titanium gettering

of the torus is carried out before every tokamak shot resulting in a low particle recycling coefficient during the discharge.

During all ECRH experiments on CLEO the RF power was transmitted up to the torus from the low-field side in oversized waveguide aligned along a major radius in the tokamak mid-plane. A directed spectrum (i.e. with finite net $k_\parallel$) required for current drive was achieved in a number of ways. At 60 GHz a Vlasov-type antenna was fed with the TE_{02} mode propagating in 30 mm diameter circular guide. This antenna produced a narrow crescent-shaped beam at 22° to the waveguide axis (Fig 1). The theoretical pattern was confirmed in both low and high power tests. The high power tests were carried out using a real-time, temperature-analysing, infra-red camera to look at the result of launching the gyrotron output onto large absorbent tiles [14]. At low power the polarisation was demonstrated to be azimuthal with respect to the waveguide axis in accordance with theory. Therefore it is to be expected that in the plasma the extraordinary mode is predominantly excited. At a distance of 15 cm the full 3dB width of the antenna pattern in the tokamak mid-plane was measured to be only 2.5 cm. Calorimetric measurements showed that up to 185 kW of RF power could be delivered to this antenna from a single 200 kW gyrotron located 32 metres away. This performance was achieved as a result of careful design of the three bends and two mode convertors incorporated in the transmission line. As a control experiment a symmetric (with respect to $k_\parallel$) spectrum was also launched into CLEO by feeding a conventional

straight-waveguide antenna with the TE_{01} mode. This produced a hollow cone pattern with the main lobe at ~12° to the waveguide axis. It is expected that in this case there is equal excitation of the extraordinary mode and the ordinary mode in the plasma.

At 28 GHz a directed wave spectrum was produced in two different ways. First of all a TE_{02} Vlasov-type antenna was employed, as at 60 GHz, but in 40 mm diameter waveguide giving a crescent-shaped antenna pattern at ~37° to the waveguide axis. Again it is to be expected that predominantly the X-mode is excited in the plasma with this antenna. Secondly a directed spectrum was achieved by launching a TE_{01}+ TE_{11} mode mixture from open-ended straight circular waveguide. The open end of a circular waveguide excited in the TE_{11} mode radiates a linearly polarised beam with its peak intensity on the waveguide axis. For 28 GHz and a waveguide diameter of 40 mm the H-plane antenna pattern has 10 dB points at ± 17°. When the same waveguide is excited in the TE_{01} mode the antenna pattern is a hollow cone with its maximum at 19° from the axis. The polarisation is azimuthal and hence the electric fields have opposite signs on either side of the waveguide axis in the tokamak midplane. If the two modes are combined the TE_{01} wave will increase the TE_{11} field on one side of the axis and decrease it on the other side as illustrated schematically in Fig 2. A mixture of TE_{01} and TE_{11} was produced by removing one period from a four-period mode convertor designed for complete $TE_{01} \rightarrow TE_{11}$ conversion. The relative phase of the two modes varies continuously in the plain waveguide following the

convertor. The deflection of the wavefront was optimised empirically by varying the length of plain 40 mm diameter waveguide between the convertor and the plasma. The angle of deflection was measured by launching the wave at high power into free space and measuring the antenna pattern with heat sensitive paper. The beam can then be directed either parallel or anti-parallel to the plasma current by rotating the convertor by 180°. In the best case, angles of +11.3° and -8.0° with respect to the waveguide axis in the tokamak mid-plane were achieved, the asymmetry being due to residual spurious modes. The radiation is almost linearly polarised and should predominantly excite the extraordinary mode in the plasma.

3. 60 GHZ EXPERIMENTS

3.1 Gross Features

A typical set of oscillograms for a 10 kA discharge is presented in Fig 3 to illustrate the parameter regime in which the experiments were conducted. The magnetic field corresponding to second harmonic cyclotron resonance at 60 GHz is 1.072T and the low-density extraordinary mode cut-off is at $n_e = n_c \sim 2.24 \times 10^{19} m^{-3}$. The ordinary mode can propagate at densities up to $2 n_c$ but absorption of this mode is weak at the second harmonic. Most of the experimental work was carried out at line-averaged densities of $\bar{n}_e \sim 4 \times 10^{18} m^{-3}$ since this

represents a satisfactory compromise between the requirements for large RF driven current (i.e. low $\bar{n}_e$) and high single-pass absorption (i.e. high $\bar{n}_e$). At this line-averaged density, the central density in the initial OH target plasma is estimated to be $n_{eo} \sim 8 \times 10^{18} m^{-3}$ (see below) which is sufficiently far below n_c to avoid strong refraction. If the gas influx, Γ, is maintained constant during the discharge there is a significant decrease in $\bar{n}_e$ during the ECRH pulse due to both a broadening of the density profile and a decrease in the total number of particles. This phenomenon has been observed in many devices [15-17] but is particularly pronounced in CLEO because of the low particle recycling coefficient of the gettered vacuum vessel walls. For discharges during which Γ is maintained constant, the decrease in $\bar{n}_e$ due to the RF increases with increasing target $\bar{n}_e$ so that the phenomenon resembles a density "clamp". Such behaviour has also been reported in the THOR tokamak [18]. During the current drive experiments described here $\bar{n}_e$, measured along a central ($R=R_0$) chord, was normally feedback controlled to be maintained approximately constant during the discharge. There is thus an increase in gas influx during RF injection and a broadening of the density profile is observed. For example with reference to the discharge shown in Fig 3, although $\bar{n}_e$ at $R=R_0$ is maintained constant (Fig 3(c)) at $\sim 4 \times 10^{18}$ m^{-3}, simultaneous off-axis interferometric measurements show that,

assuming a profile family of the form $n_e = n_{eo} (1-r^2/a^2)^{\alpha_n}$, n_{eo} decreases from $\sim 8 \times 10^{18}$ m^{-3} to $\sim 6 \times 10^{18}$ m^{-3} whilst α_n decreases from ~ 2.6 to ~ 1.6 upon RF injection. The total number of electrons is not significantly changed but of course the increase in Γ implies a significant reduction in the global particle confinement time τ_p. The "overshoot" in $\bar{n}_e$ at the end of the RF pulse is evidence that τ_p recovers as soon as the RF is turned off.

Pulse height analysis of the soft X-ray emission spectrum measured with a Si(Li) detector before and during RF injection typically indicates an increase in central electron temperature from $T_{eo} \sim 400 \pm 50$ eV to $\sim 1250 \pm 200$ eV upon injection of 185 kW of RF power. In contrast to earlier low density experiments at 28 GHz [19] there is no strong tail formation either during the OH phase or the RF phase of the discharge although a soft tail is observed (Fig 4). The experimentally measured spectra at both 28 GHz and 60 GHz have been successfully modelled using a bounce-averaged Fokker-Planck code [20]. A hard X-ray detector located outside the 25 mm thick stainless steel vacuum vessel detects emission arising from the slowing down of electrons with energies $E \gtrsim$ 100 keV in the tungsten limiters or vacuum vessel wall. The low level of emission present in the initial OH phase is normally extinguished by the RF (Fig 3(d)). This is possibly associated with the strong reduction in the DC electric field but may also indicate that the fast electron confinement is influenced by the RF. The reappearance, or

not, of the emission after the RF pulse depends strongly on the plasma density behaviour during this phase of the discharge. For the usual conditions shown in Fig 3 there is little emission during or after the RF.

It should be noted that in these low current (typically $I_p \sim 10$ kA) plasmas, estimates of the RF absorption efficiency (see below) indicate that P_{RF}(absorbed)$/P_{OH}$(initial) $\gtrsim 10$ whilst the ohmic power input is completely negligible during the RF phase. Magnetic measurements indicate that the poloidal beta, β_p, increases from ~ 0.7 to ~ 2.7 upon RF injection. If a temperature profile of the form $T_e = T_{eo}(1-r^2/a^2)^{\alpha_T}$ is assumed these measurements are consistent with the interferometric density measurements and the Si(Li) measurements of T_{eo} if α_T decreases from ~ 4.2 to ~ 2.1 upon injection of RF. The broadening of $T_e(r)$ and $n_e(r)$ is reflected in the strong broadening of the soft X-ray emission profile, $I_{SXR}(r)$, as measured with an array of surface barrier diodes viewing the plasma from above (Fig 5). Furthermore, it can be seen that accompanying the large increase in absolute emission (Fig 3 (g)) there is a strong outward shift in peak emission upon RF injection (Fig 5) associated with the large increase in β_p. Note that the excursion in the position of the outermost flux surface is held to a small value (Fig 3(f)) by the position feedback control system.

The parameters (typical) during the OH phase and the RF phase of the discharge in Fig 3 are summarised in Table I. The total power input during the RF phase is calculated using the estimated absorption efficiency of ~ 80-85% (see Fig 10 and associated discussion) combined with the measured injected power (185 kW). The energy confinement time degrades in an L-mode-like manner falling in this case to ~ 0.9 ms which lies between the predictions of the Goldston [21] and the Kaye-Goldston [22] scaling laws which give $\tau_E \sim$ 1.6 ms and $\tau_E \sim$ 0.5 ms respectively. It should be further noted that during the RF phase $\beta \sim \beta_p(\varepsilon/q(a))^2 \sim 0.06\% \sim 0.3\beta_{crit}$ where β_{crit} is the critical beta given by Troyon et al [23].

Evidence that the broadening in $n_e(r)$ and $T_e(r)$ is accompanied by a broadening in the current profile $j(r)$ is provided by the observation of sawtooth stabilisation. Figure 6 shows that for the discharge illustrated in Fig 3 the sawtooth activity disappears shortly after the onset of ECRH although it reappears in the form of rounded sawteeth several milliseconds later. The presence of sawteeth in the initial ohmic phase indicates a very peaked current profile in view of the very high q at the edge, viz q(a) ~ 10. Figure 7, for a 15 kA discharge, shows complete stabilisation of sawteeth during the ECRH phase with their reappearance after the RF. The sawtooth period is typically between 0.5 and 1.0 ms but this increases to over 2 ms when the resonance position is displaced outwards by ~ 4 cm ie, close to the shifted magnetic axis (Fig 5). This is probably associated with the

deposition profile being centred accurately inside the q=1 surface. As at 28 GHz no slow precursor activity is apparent before the sawtooth crash.

3.2 Current Drive Studies

For discharges studied initially (such as that in Fig 3) the plasma current flowed in a counterclockwise (CCW) direction and the waves were launched preferentially in a clockwise (CW) direction around the torus, as viewed from above. Since the waves were injected from the low-field side, and bearing in mind the relativistic effects on the resonance condition pointed out by Cairns et al [8], this is expected to lead to an RF driven current which is parallel to the existing ohmically driven current; ie since

$$\omega - \ell\omega_{ce}/\gamma = k_{\parallel}v_{\parallel} > 0$$

the waves are expected to drive an electron current in the same direction as the wave propagation. The wavenumber and electron velocity components parallel to the magnetic field are denoted by $k_{\parallel}$ and $v_{\parallel}$ respectively, ω is the angular frequency of the wave, ω_{ce} ($\equiv$ eB/m) is the electron cyclotron frequency, $\gamma(\equiv(1 - v^2/c^2)^{-\frac{1}{2}})$ is the relativistic factor and the equation applies at the ℓth harmonic. It is not possible to open-circuit the primary in CLEO during the discharge and the loop voltage was not driven to zero or below with the

available RF power. However since the plasma current can be held
closely constant using a fast feedback amplifier it is possible to
identify non-inductive currents by measuring the difference in loop
voltage, V_ℓ, when the relative direction of $\underline{k}$ is reversed with respect
to I_p. A clear and consistent difference in loop voltage was observed
in the 60 GHz experiments whether the current or antenna direction was
changed.

Rotation of the Vlasov antenna in order to reverse the direction of $\underline{k}$
involved a significant perturbation to the 30 m RF transmission line.
Therefore, in the first instance, I_p was reversed. The loop voltage
waveforms for discharges with CW and CCW plasma currents ($\underline{k}$ is CW) are
shown in Fig 8. There is a substantial difference in V_ℓ during the RF
phase although in all other respects, for example the line-averaged
density, stored energy (diamagnetic measurements) and electron
temperature (Si(Li) detector measurements) the discharges were
virtually identical. Furthermore the absolute soft X-ray emission and
its profile $I_{SXR}(r)$, which is particularly sensitive to T_e and n_e, was
the same for both discharges. The variation of V_ℓ was studied as a
function of B_ϕ (ie, as a function of resonance position) for both
directions of I_p (Fig 9). If it is assumed that the RF driven
component of the plasma current, I_{RF}, is unchanged when I_p is reversed
and that the plasma resistance is the same in both cases one may
write,

$$I_p - I_{RF} = V_{CCW}/R_p$$

and
$$I_p + I_{RF} = V_{CW}/R_p$$

Thus,

$$I_{RF} = \frac{(1-V_{CCW}/V_{CW})I_p}{(1+V_{CCW}/V_{CW})} \tag{1}$$

where V_{CCW} and V_{CW} are the loop voltages measured with counterclockwise and clockwise plasma currents respectively and R_p is the plasma resistance. The RF driven current deduced in this way from Fig 9 is plotted as a function of toroidal field in Fig 10. Also displayed in this diagram are the experimental estimates of absorption efficiency which were obtained by estimating the unabsorbed gyrotron power using a calibrated 'horn receiver' to detect the magnitude of 60 GHz radiation in the torus. The absorbed power was typically 80-90% and only a weak function of B_ϕ, I_p and $\bar{n}_e$. This confirms the theoretical prediction that wall reflections may ensure efficient absorption even when the single pass absorption decreases significantly.

The deduced RF driven current was found to increase with I_p in the range 5 kA $\leq I_p \leq$ 15 kA (Fig 11). Also displayed in this diagram, for comparison, is the RF driven current in a 10 kA discharge for an injected RF power of 120 kW. It was not possible to study the

variation of I_{RF} with P_{RF} over a significantly wide range since the 60 GHz gyrotron did not operate reliably below an output level of ~ 100 kW. Similarly, because of the difficulties of particle control discussed in section 3.1, in particular the "density clamp" effect of the RF, it was not possible to study the current drive efficiency as a function of $\bar{n}_e$.

A second experimental campaign was carried out with the Vlasov antenna rotated through 180 degrees to launch waves with $\underline{k}$ CCW. As before, experiments were carried out with CW and CCW plasma currents and the results were compared. In Fig 12(a) the loop voltage measured during ECRH with P_{RF} = 185 kW is plotted as a function of B_ϕ for both directions of plasma current. Once again there is a significant difference in V_ℓ between the two directions of I_p but comparison with Fig 9 shows that upon rotation of the antenna the lower loop voltage is achieved with I_p CW instead of I_p CCW. This rules out the suggestion that the difference in V_ℓ for the discharges shown in Fig 8, for example, is due to some device asymmetry with respect to the direction of I_p, [24-25]. Unfortunately the RF heating obtained during the B_ϕ scans used in Fig 12(a) was not the same for the two directions of I_p for reasons which we have been unable to ascertain. This is illustrated in Fig 12(b) where the increase in poloidal beta during ECRH is plotted against B_ϕ. Although this complicates the quantitative

analysis, examination of Figs 12(a), 12(b) provides clear, unequivocal evidence of a non-inductive component of the plasma current when the following points are noted:

(i) For I_p CCW and B_ϕ = 1.034 T, $\Delta\beta_p \sim 1.4$ and $V_\ell \gtrsim 0.5$ V yet for I_p CW and B_ϕ = 1.005 T, V_ℓ is only ~ 0.25 V even though $\Delta\beta_p < 0.6$.

(ii) For I_p CCW and B_ϕ = 1.1 T strong heating is observed with $\Delta\beta_p \sim$ 2.2-2.4. At the same field, but with I_p CW, much lower heating ($\Delta\beta_p \lesssim 1.2$) was observed yet the same loop voltage (~ 0.4 V) was measured. At lower B_ϕ (~ 1.07 T) when the same heating efficiency was achieved ($\Delta\beta_p \sim 2.3$) a loop voltage of only 0.1-0.15 V was measured for I_p CW.

(iii) With the TE_{01} launch, when no net RF driven current is expected, heating experiments were also carried with both directions of I_p. For I_p CW exceptional heating was observed with $\Delta\beta_p \sim 3.3$ (implying $\beta_p \sim 4$, i.e. $\epsilon\beta_p > 0.5$). Electron cyclotron emission and Si(Li) detector measurements indicated that the central electron temperature was increased to ~ 2 keV. The reason for this has not been determined. A loop voltage of ~ 0.1-0.15 V was measured ie, of the same order as with the directed launch when $\Delta\beta_p \sim 2.3$ was measured. In fact for I_p CCW and TE_{01} launch $\Delta\beta_p \sim$ 2.2-2.3 was obtained but in this case $V_\ell \sim 0.25$ V. The difference in V_ℓ for different I_p directions when using the TE_{01} launch is explicable, within the experimental errors, in terms

of the different heating observed. In fact it should be
mentioned that in 15 kA discharges using the TE_{01} launch the
same $\Delta\beta_p$ and the same V_ℓ were achieved for both I_p directions.

One may gain further insight by concentrating only on data from Fig 12
for which $\Delta\beta_p \sim 2.3$ (ie $\beta_p \sim 3$). This data is summarised in Table II.
For the TE_{02} discharges one can then write

$$I_p - I_{RF} = V_{CW}/R_p$$

and
$$I_p + I_{RF} = V_{CCW}/R_p$$

where I_p = 10 kA, $V_{CW} \sim 0.125$ V, V_{CCW} = 0.4 V and I_{RF} and R_p are
assumed to be the same in each case since $\Delta\beta_p$ is the same. Solution of
these equations gives

$$I_{RF} \sim 5.2 \text{ kA}$$

and,

$$R_p \sim 26 \ \mu\Omega$$

(NB Assuming Spitzer resistivity with a temperature profile
$T_e = T_{eo}(1 - r^2/a^2)^2$ and Z_{eff} = 2 this would imply $T_{eo} \sim 950$ eV)

For the TE_{01} mode one may write

$$I_p = V_\ell / R_p$$

which would predict (taking the same R_p)

$$V_\ell \sim 0.26 \text{ V}$$

in close agreement with experiment.

It can be clearly seen in Fig 12(b) that there is a strong asymmetry in heating efficiency with respect to the resonance position relative to the torus minor axis. As the resonance moves to larger major radii the heating efficiency falls off extremely rapidly for $R > R_0$. This behaviour has been reported previously at 28 GHz in CLEO [15] and has also been observed in WT-2 [11]. In the case of the CLEO experiments there is evidence from soft X-ray and electron cyclotron emission measurements to suggest that this phenomenon is connected with wave coupling to trapped electrons which are then rapidly lost [26].

4. 28 GHZ EXPERIMENTS

The extraordinary mode cut-off density for 28 GHz second harmonic heating is at $n_c \sim 4.85 \times 10^{18}$ m^{-3}. The heating efficiency falls substantially if n_{eo} significantly exceeds n_c since wave absorption is

restricted to the outer regions of the plasma. Therefore most experiments at 28 GHz were carried out at a line-averaged density of $\bar{n}_e \sim 2 \times 10^{18}$ m^{-3}. A typical discharge is illustrated in Fig 13. With I_p = 10 kA (feedback controlled) and CCW, the Vlasov antenna was rotated to launch waves both CW and CCW. The toroidal field was varied around the second harmonic resonant value of 0.50 T for both antenna orientations. In Fig 14, where the loop voltage and the increase in poloidal beta due to the RF are plotted as a function of B_ϕ, it is seen that in contrast to the experiments at 60 GHz there are no significant differences for the two antenna orientations. The injected power was measured calorimetrically to be 120 kW, exceeding the initial ohmic power by almost an order of magnitude. For central heating ($B_{\phi 0} \sim 0.5$. T) $\Delta\beta_p \sim 1$ and as observed at 60 GHz the heating efficiency falls off rapidly for $B_{\phi 0}$ greater than the resonant value.

Closer examination of the diagnostic behaviour for the two antenna orientations (eg soft X-ray profiles, sawtooth behaviour, hard X-ray emission etc) fails to reveal any discernible differences. At such low densities, sawteeth are normally absent in the ohmic phase (despite q(a) $\sim$ 5 ie, a factor of two lower than in the 60 GHz experiments). However injection of RF often results in the excitation of sawteeth. As at 60 GHz the hard X-ray emission ($\gtrsim$ 100 keV) is usually extinguished by the RF and increased gas influx is required during the RF phase to maintain $\bar{n}_e$ constant. As $\bar{n}_e$ is increased, sawteeth appear

in the ohmic phase and the hard X-ray emission falls to a negligible level before and during the RF. However, in such discharges a large spike of hard X-ray emission is usually observed , 5-6 ms after termination of the RF. This would indicate that despite the low overall heating efficiency observed for $\bar{n}_e \sim$ 3-4 x 10^{18} m^{-3} the RF can still accelerate electrons to energies in excess of 3-4 keV which can then 'runaway' in the post-RF electric field ($\sim$ 0.4 V/m). The time-delay between RF turn-off and appearance of the X-ray burst is consistent with this mechanism.

Experiments were also carried out using the TE_{01} + TE_{11} mode mixture described in section 2. In this case the RF was injected into discharges with decaying plasma current. The inductance in the primary circuit was reduced to a low value to accentuate changes in I_p and dI_p/dt as a result of RF heating and current drive. The voltage and current waveforms for two discharges into which the RF waves were launched CW and CCW respectively are shown in Fig 15. The plasma current is CW and is $\sim$ 10 kA at the time of injection. The injected power was 135 kW. There is no significant difference between the two sets of oscillograms.

5. THEORETICAL MODELLING

Theoretical studies of the absorption and the expected RF driven current have been carried out using a ray tracing code which includes a current drive model allowing for trapping effects [27] and the weakly relativistic resonance condition [28]. Predictions of current drive by a bounce-averaged Fokker-Planck code [20,29] agree well with the linear current drive calculations. In addition, the electron distribution function predicted by the code is consistent with the measured X-ray spectrum during ECRH.

The 60 GHz radiation pattern shown in Fig 1 was modelled by a bundle of 270 rays. Profiles of the form $n_e = n_{eo} (1-r^2/a^2)^2$ and $T_e = T_{eo} (1-r^2/a^2)^3$ and shifted flux surfaces with the magnetic axis displaced by up to 4 cm were assumed in accordance with the experimental data. The results are illustrated in Fig 10. Multiple wall reflections are included in the calculations although for central heating and current drive this has little effect since the single pass absorption is $\sim 80\%$. As the resonance is moved off-axis wall reflections play a more important role enabling the high absorption efficiencies of $\gtrsim 80\%$ to be maintained in agreement with the experimental measurements. However the RF driven current falls off much more strongly as $B_{\phi o}$ is varied since multiple passes of the waves through the resonant region produce strong cancellation effects of the

oppositely driven currents on either side of the resonance. This prediction is also in accord with the experimental results.

However, although the calculations are able to correctly predict the absorption efficiency and the scaling of the absorption and of the RF driven current with $B_{\phi 0}$, the absolute magnitude of I_{RF} is overestimated by a factor $\sim$ x 3. The theoretical results shown in Fig 10 already include the effect of electron trapping which reduces the predicted current by typically $\sim$ 20% for the cyclotron resonance at $R \lesssim R_0$. As $B_{\phi 0}$ is raised so that the resonance is displaced outwards to $R > R_0$ the calculations show that the trapping effects are severe, reducing I_{RF} by a factor of $\gtrsim$ 2. The theoretically predicted current drive efficiency for central resonance is $\sim$ 70 A/kW launched, corresponding to a figure of merit $\eta \equiv \bar{n}_e \ (10^{20} \ m^{-3}) \ I_{RF} R_0 / P_{RF} \sim 2 \times 10^{-3}$. This figure is low compared with that achieved in LHCD experiments because, as Fokker-Planck calculations have shown, the waves interact primarily with electrons in the range $1 \lesssim v_\parallel / v_e \lesssim 2$, where v_e is the electron thermal velocity. In all LHCD experiments in which efficient current drive has been achieved, high phase velocity waves have been launched in order to interact with very energetic electrons. As with LHCD, the ECRH current drive efficiency increases strongly with increasing $v_\parallel / v_e$ [27]. The Fokker-Planck calculations also show that distortion of the electron distribution function from Maxwellian by the ECRH is significantly less in the conditions of the 60 GHz experiments than in those of the 28 GHz experiments [20].

The calculated profiles of absorbed power and of RF driven current are shown in Fig 16. As the heating and driven current profiles are somewhat broader than the high q displaced ohmic profiles, sawtooth suppression is to be expected, as observed experimentally (Figs 6,7). However it would appear that the sawtooth activity is more sensitive to the absorption profile and its location than the current drive profile since no significant difference in sawtooth activity is observed between co- and counter-current-drive and since stabilisation is normally achieved on a very rapid timescale (within one sawtooth period after RF switch-on).

The possible influence of a bootstrap current [30] has been studied. Employing the transport coefficients given by Hinton and Hazeltine [31] the current density arising from the bootstrap effect is given by

$$j_{BS} = -e(r/R)^{\frac{1}{2}} \left[2.33 \, T_e(eV) \frac{dn_e}{dr} + 0.74 \, n_e \frac{dT_e(eV)}{dr} \right]/B_\theta$$

For these hot electron plasmas with $\nu_e^* \sim 0.1$ over most of the plasma profile and poloidal beta values up to 3 the bootstrap current is calculated to be between 4 kA and 7 kA with a hollow profile peaked at ~ 4 cm from the magnetic axis (Fig 16). The expected bootstrap current in the initial ohmically heated plasma is much smaller ($\lesssim 2$ kA). The presence of such a bootstrap current in the RF phase of the discharge would lead to a significant reduction in our estimates of I_{RF} since one

-22-

should replace I_p in equation (1) by $(I_p - I_{BS})$ where I_{BS} is the bootstrap current. However, the appearance of such a hollow profile bootstrap current should not only suppress sawtooth activity in these high q discharges but should also initially depress the loop voltage significantly below zero when the RF driven component is parallel to the inductively driven current (and hence also to I_{BS}) as indicated in Fig 8 from current diffusion calculations carried out using the HERMES code [32]. No transient decrease in loop voltage is seen associated with the predicted decrease in inductance. Furthermore, neglecting the bootstrap effect the current diffusion calculations show that within errors the average of the loop voltage decreases observed for co- and counter-current-drive corresponds to the observed temperature rise if the resistivity remains neo-classical and Z_{eff} remains close to 2. It is possible that the effect of a bootstrap current could be masked by an enhancement of the resistivity by trapped electron effects over and above that given by the usual neo-classical expressions and brought about by the wave interaction. However the transient loop voltage behaviour should still be evident. Therefore it would appear that the bootstrap current is much smaller than theoretically predicted in these plasmas.

6. DISCUSSION AND SUMMARY

The conflict between theory and experiment evident in the results presented here requires some discussion. In particular the reduced

current drive efficiency at 60 GHz and the complete absence of RF driven current at 28 GHz need explanation. Ray tracing calculations suggest that similar current drive efficiencies should be achieved in the 28 GHz and 60 GHz experiments. It is possible that the resolution of our dilemma may be associated with the relative timescales involved. The Fisch-Boozer mechanism of ECRH current drive relies upon collisional relaxation of the heated electrons upon the background ions to establish the RF driven current via the asymmetric resistivity effect. This relaxation may occur directly or via interaction first with the background electrons. In either case additional energy losses from the electron population, and particularly from the resonant electrons, will interfere with the current drive mechanism. Such effects may be especially important in conventional ECRH where the resonant electrons are more closely tied to the bulk than in LHCD for example. As a consequence the resonant electrons are unlikely to be immune from the anomalous processes known to strongly influence the global energy confinement in ohmically heated plasmas or the effects associated with auxiliary heating which lead to a further deterioration in the overall confinement. As already pointed out, in the experiments described here, both the global energy and particle confinement times are observed to decrease upon RF injection.

Fokker-Planck calculations suggest that the energy of resonant electrons is ~3-4 keV in these experiments. For the conditions of the 60 GHz (28 GHz) experiments such electrons have an electron-electron

collision time, τ_c, [31] of order 1 ms (2 ms) whilst the electron-ion collision time is of the same order or a little shorter for the estimated Z_{eff}. Fokker-Planck calculations confirm that the RF driven current is established on a timescale of the order ~2-3 τ_c as shown in Figure 17. In the case of the 60 GHz experiments $\tau_c \sim \tau_E$, the global energy confinement time, (see Table I) whilst it is estimated that $\tau_c \sim$ 4 τ_E for the 28 GHz discharges. Thus in the present experiments the collisional slowing down time for the resonant electrons is of the same order as (60 GHz), or significantly longer than (28 GHz), the experimental energy confinement time. In such circumstances the observed results may be understandable. It should be noted that the processes responsible for the short confinement time may also inhibit the establishment of the bootstrap current.

In summary, second harmonic electron cyclotron current drive has been demonstrated at 60 GHz in the CLEO tokamak. The mechanism clearly differs from that observed in the WT-2/WT-3 experiments which relies upon interaction with a strong established electron tail. A decrease in energy and particle confinement and a modification of the sawtooth activity accompanies RF injection. The scaling of the RF absorption and of the RF driven current with toroidal magnetic field (and therefore with resonance position) is in agreement with theory. The low current drive efficiency observed at 60 GHz and the absence of RF driven current at 28 GHz may be associated with the fact that the collisional slowing down time of the resonant electrons is of the same order or longer than the global energy confinement time together with the fact that the resonant electrons remain closely tied to the bulk

distribution and are therefore unlikely to be immune from the anomalous loss processes which determine τ_E. Finally, it would appear that in these experiments the bootstrap current is either absent or much smaller than theoretically predicted.

ACKNOWLEDGEMENTS

REFERENCES

[1] PORKOLAB, M., in Wave Heating and Current Drive in Plasma, Ed. Granatstein, V. L. and Colestock, P. L., Gordon and Breach, New York (1985) 219, and references therein.

[2] FISCH, N. J., Phys. Rev. Lett. 41 (1978) 873.

[3] KARNEY, C. F. F. and FISCH, N. J., Phys. Fluids 22 (1979) 1817.

[4] CORDEY, J. G., EDLINGTON, T. and START, D. F. H., Plasma Phys. 24 (1982) 73.

[5] FISCH, N. J., Rev. Mod. Physics 59 (1987) 175, and references therein.

[6] WONG, K. L. and ONO, M., Nucl. Fusion 24 (1984) 615.

[7] FISCH, N. J. and BOOZER, A. H., Phys. Rev. Lett. 45 (1980) 720.

[8] CAIRNS, R. A., OWEN, J., and LASHMORE-DAVIES, C. N., Phys. Fluids 26 (1983) 3475.

[9] START, D. F. H., AINSWORTH, N. R., CORDEY, J. G., EDLINGTON, T., FLETCHER, W. H. W., PAYNE, M. F. and TODD, T. N., Phys. Rev. Lett. 48 (1982) 624.

[10] ALCOCK, M. W., LLOYD, B., MORRIS, A. W., ROBINSON, D. C. and START, D. F. H., in Plasma Physics and Controlled Nuclear Fusion Research (Proc 9th Int. Conf. Baltimore, 1982), Vol. 2, IAEA, Vienna (1983) 51.

[11] ANDO, A., OGURA, K., TANAKA, H., IIDA, M., IDE, S., OHO, K., OZAKI, S., NAKAMURA, M., CHO, T., MAEKAWA, T., TERUMICHI, Y. and TANAKA, S., Phys. Rev. Lett. 56 (1986) 2180.

[12] TANAKA, S., TERUMICHI, Y., MAEKAWA, T., NAKAMURA, M., ANDO, A., OGURA, K., TANAKA, H., IIDA, M., IDE, S., OHO, K., OZAKI, S., IWAMURA, K., YAMAZAKI, A. and TAKASE, H., in Controlled Fusion and Plasma Physics (Proc. 14th Eur. Conf. Madrid, 1987), Vol. 3, European Physical Society (1987) 886.

[13] REYNOLDS, P., MILLWARD, P. and HUNT, R. R., in Plasma Physics and Controlled Nuclear Fusion Research (Proc. 5th Int. Conf. Tokyo, 1974), Vol. 2, IAEA, Vienna (1975) 13.

[14] ROBINSON, D. C., AINSWORTH, N. R., COLLINS, P. R., DELLIS, A. N., EDLINGTON, T., HAYNES, P. S., IYENGAR, S., JOHNSON, I., LLOYD, B.,

O'BRIEN, M., PARHAM, B. J., RIVIERE, A. C., START, D. F. H. and
TODD, T. N., in Plasma Physics and Controlled Nuclear Fusion
Research (Proc. 11th Int. Conf. Kyoto, 1986), Vol. 1, IAEA,
Vienna (1987) 575.

[15] EDLINGTON, T., ALCOCK, M. W., ATKINSON, D., BLEWETT, S. G.,
PARHAM, B. J., COLLINS, P. R., DELLIS, A. N., LLOYD, B., O'BRIEN,
M., RILEY, J., RIVIERE, A. C., ROBINSON, D. C., START, D. F. H.
and TODD, T. N., in Controlled Fusion and Plasma Heating (Proc.
13th Eur. Conf. Schliersee, 1986), Vol. 2, European Physical
Society (1986) 219.

[16] T-10 GROUP, in Controlled Fusion and Plasma Physics (Proc. 12th
Eur. Conf. Budapest, 1985), Vol. 1, European Physical Society
(1985) 38.

[17] LaHAYE, R. J., MOELLER, C. P., FUNAHASHI, A., YAMAMOTO, T.,
HOSHINO, K., SUZUKI, N., WOLFE, S. M., EFTHIMION, P. C., TOYAMA,
H. and ROH, T., Nucl. Fusion $\underline{21}$ (1981) 1425.

[18] ARGENTI, L., CIRANT, S., MANTICA, P. and TARTARI, U., in
Controlled Fusion and Plasma Physics (Proc. 14th Eur. Conf.
Madrid, 1987) Vol. 3, European Physical Society (1987) 819.

[19] ROBINSON, D. C., AINSWORTH, N. R., ALCOCK, M. W., ATKINSON, D., COLLINS, P. R., DELLIS, A. N., EDLINGTON, T., FERREIRA, A., GAO, Q., HENDER, T. C., MA, Z., MORRIS, A. W., O'BRIEN, M., PARHAM, B., RIVIERE, A. C., START, D. F. H., TAKAMURA, S. and TODD, T. N., in Plasma Physics and Controlled Nuclear Fusion Research (Proc. 10th Int. Conf. London, 1984), Vol. 1, IAEA, Vienna (1985) 205.

[20] O'BRIEN, M. R., COX, M and START, D. F. H., Computer Physics Communications 40 (1986) 123.

[21] GOLDSTON, R. J., Plasma Physics and Controlled Fusion, 26 (Spec. Issue: Proc. 11th Eur. Conf. Controlled Fusion and Plasma Physics, Aachen, 1983) (1984) 87.

[22] KAYE, S. M. and GOLDSTON, R. J., Nucl. Fusion 25 (1985) 65.

[23] TROYON, F., GRUBER, R., SAURENMANN, H., SEMENZATO, S. and SUCCI, S., Plasma Physics and Controlled Fusion, 26 (Spec. Issue: Proc. 11th Eur. Conf. Controlled Fusion and Plasma Physics, Aachen, 1983) (1984) 209.

[24] WILHELM, R., JANZEN, G., MULLER, G., SCHULLER, P. G., SCHWORER, K., THUMM, M. and ERCKMANN, V., Plasma Physics and Controlled Fusion, 26 (Spec. Issue: Proc. 11th Eur. Conf. Controlled Fusion and Plasma Physics, Aachen, 1983) (1984) 259.

[25] McLENITHAN, K. D., SHOHET, J. L. and GRIEGER, G., in Controlled Fusion and Plasma Physics (Proc. 11th Eur. Conf. Aachen, 1983), Vol. 1, European Physical Society (1983) 219.

[26] ROBINSON, D. C., in Turbulence and Transport, Ed. Gresillon, D. and Dubois, M. A., (Proc. of Int. Workshop on Small Scale Turbulence and Anomalous Transport in Magnetized Plasmas, 1986) Editions de Physique, Orsay (1987) 21.

[27] CORDEY, J. G., EDLINGTON, T. and START, D. F. H., Plasma Physics and Controlled Fusion 24 (1982) 73.

[28] FERREIRA, A., O'BRIEN, M. R. and START, D. F. H., Plasma Physics and Controlled Fusion 26 (1984) 1565.

[29] O'BRIEN, M. R., COX, M. and START, D. F. H., Nucl. Fusion 26 (1986) 1625.

[30] BICKERTON, R. J., CONNOR, J. W. and TAYLOR, J. B., Nature (London) Phys. Sci. 229 (1971) 110.

[31] HINTON, F. L. and HAZELTINE, R. D., Rev. Mod. Phys. 48 (1976) 239.

[32] HUGHES, M. H. and ARTER, W., private communication.

TABLE I

TYPICAL PLASMA PARAMETERS

I_p = 10 kA, B_ϕ = 1.07 T, f = 60 GHz

	OHMIC PHASE	RF PHASE
T_{eo}	400 eV	1250 eV
$\bar{n}_e$	$4 \times 10^{18} m^{-3}$	$4 \times 10^{18} m^{-3}$
n_{eo}	$8 \times 10^{18} m^{-3}$	$6 \times 10^{18} m^{-3}$
β_p	0.7	2.7
P_{TOTAL}(absorbed)	~ 14 kW	~ 155 kW
τ_E	~ 2.3 ms	~0.9 ms

TABLE II

COMPARISON OF LOOP VOLTAGE RESPONSE FOR
DIFFERENT MODES OF INJECTION AND PLASMA CURRENT DIRECTIONS

$$I_p = 10 \text{ kA; } P_{RF} = 185 \text{ kW; } f = 60 \text{ GHz}$$

Mode	I_p direction	B_ϕ (T)	$\Delta\beta_p$	V_ℓ (V)
TE_{02} (Vlasov)	CW	1.07	~2.3	0.1-0.15
TE_{02} (Vlasov)	CCW	1.10	~2.3	0.4
TE_{01} (Balanced)	CCW	1.07	~2.3	0.25
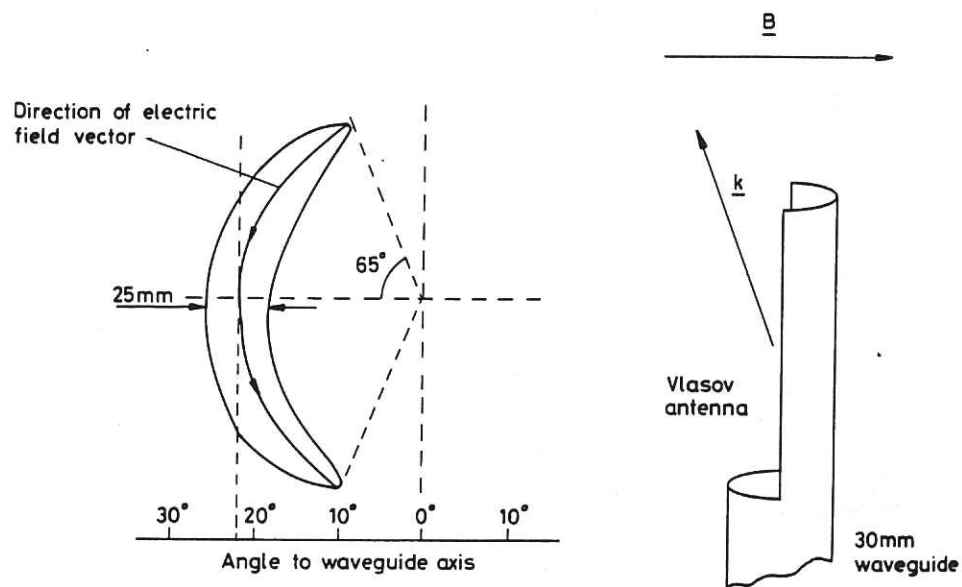
Fig. 1 Antenna pattern of the 60 GHz Vlasov antenna. The
maximum power is radiated at 22° to the waveguide axis in the
tokamak midplane. The crescent shape is the locus of the 3dB
point. The width of pattern and the angle subtended by the tips of
the crescent denoted in the diagram refer to the results of
experimental measurements made at 15 cm from the antenna.
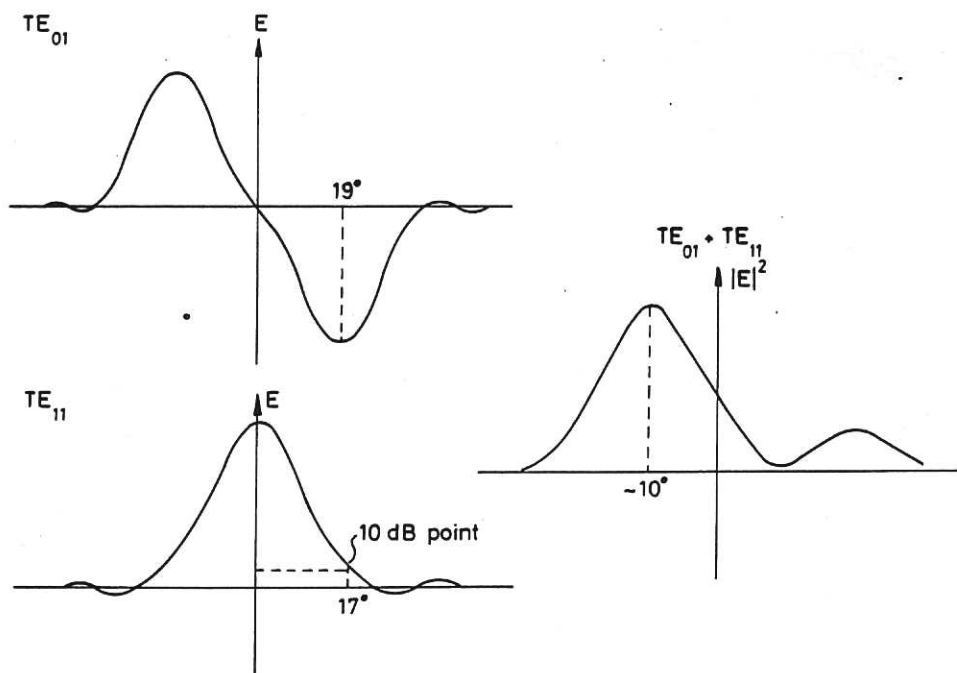
Fig. 2 Schematic illustration of the production of a directed
spectrum by means of mode mixing. E is the electric field
intensity.
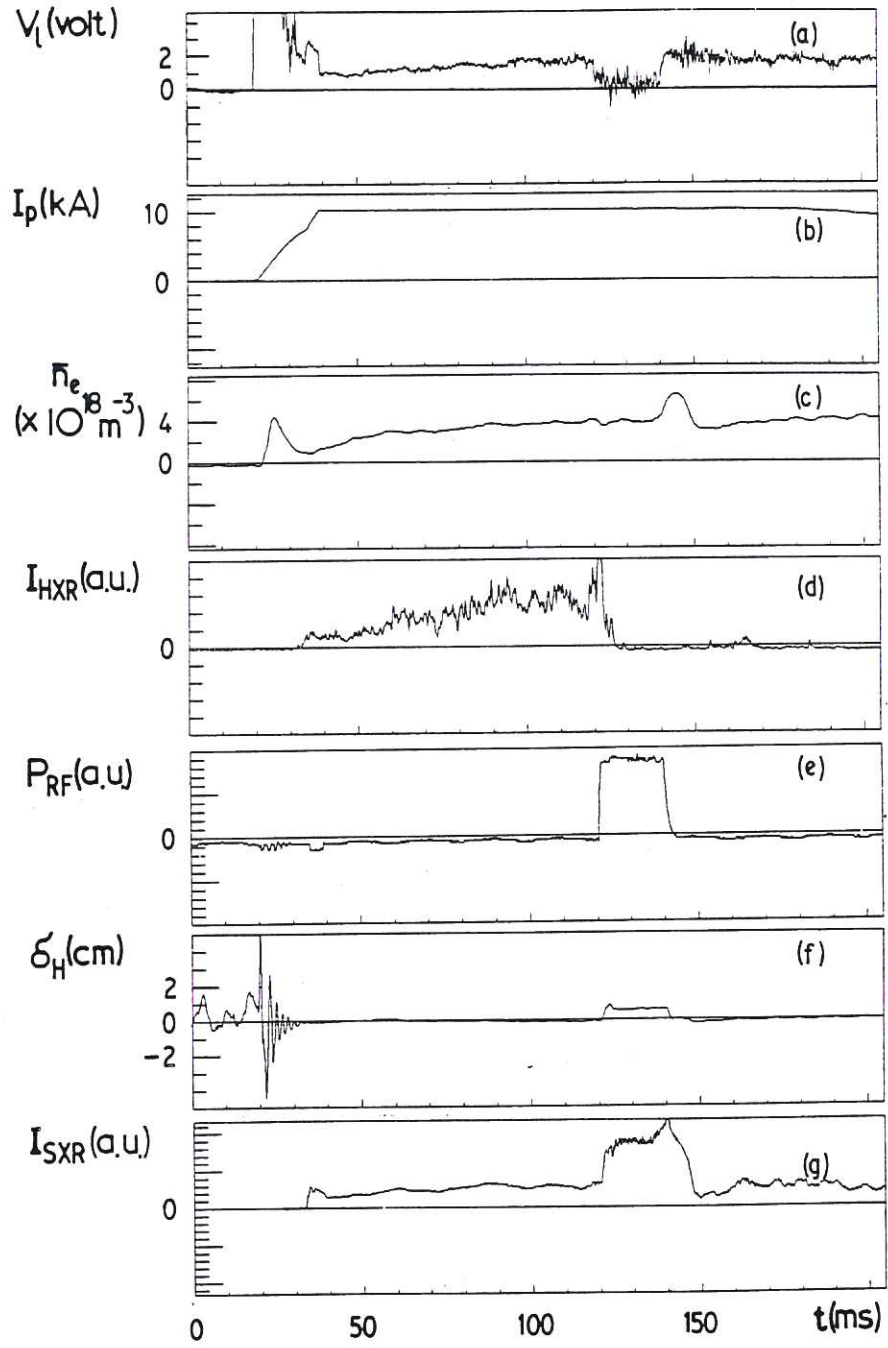
Fig. 3 A typical discharge for 60 GHz current drive studies; $B_{\phi 0} = 1.072\,\text{T}$, $P_{RF} = 185\,\text{kW}$, (a) loop voltage, V_ℓ, (b) plasma current, I_p, (c) line-averaged electron density (at $R = R_0$), $\bar{n}_e$, (d) hard X-ray emission, I_{HXR}, (e) RF power, P_{RF}, (f) in-out plasma position, δ_H, (g) line-integrated soft X-ray emission (at $R = R_0$), I_{SXR}.
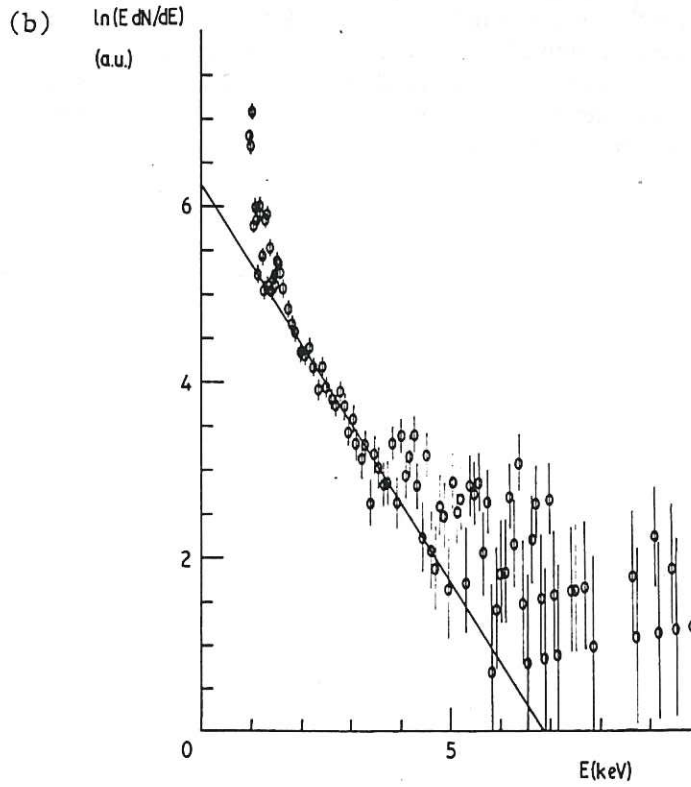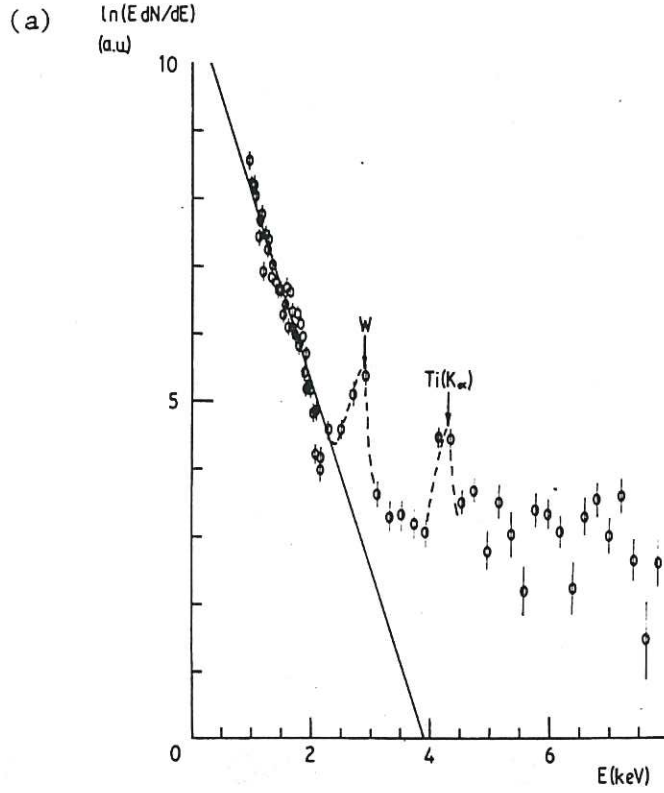
Fig. 4 X-ray emission spectra at $I_p = 10\,\text{kA}$, $\bar{n}_e \approx 4 \times 10^{18}\text{m}^{-3}$ recorded with a Si(Li) detector during (a) ohmic phase and (b) RF phase ($P_{RF} = 185\,\text{kW}$; $f = 60\,\text{GHz}$). The line-fits represent temperatures of 360 eV and 1100 eV for the ohmic and RF phases respectively.
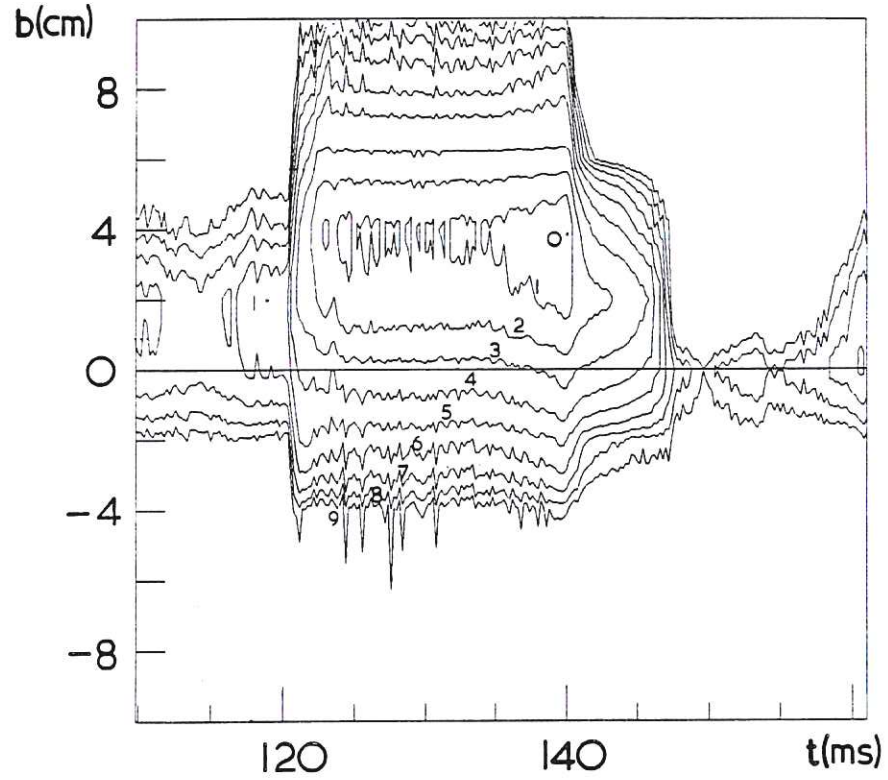
Fig. 5 Contours of constant line-integrated soft X-ray emission, I_{SXR}, for the discharge in Fig. 3, recorded with a surface-barrier diode array. Contours labelled $0, \ldots n \ldots 9$ correspond to emission levels $I_{MAX}, \ldots I_{MAX}/(1.5)^n, \ldots I_{MAX}/(1.5)^9$. b is the impact parameter of the chord to the torus minor axis (positive sign corresponds to outboard or low-field side).
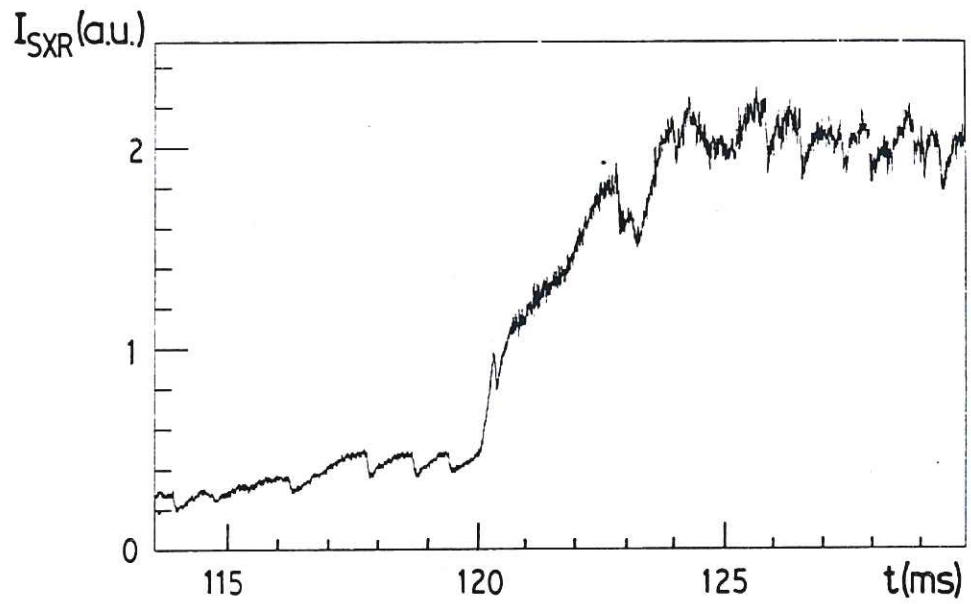
Fig. 6 Line-integrated soft X-ray emission at $b = +2$ cm for the discharge in Fig. 3.
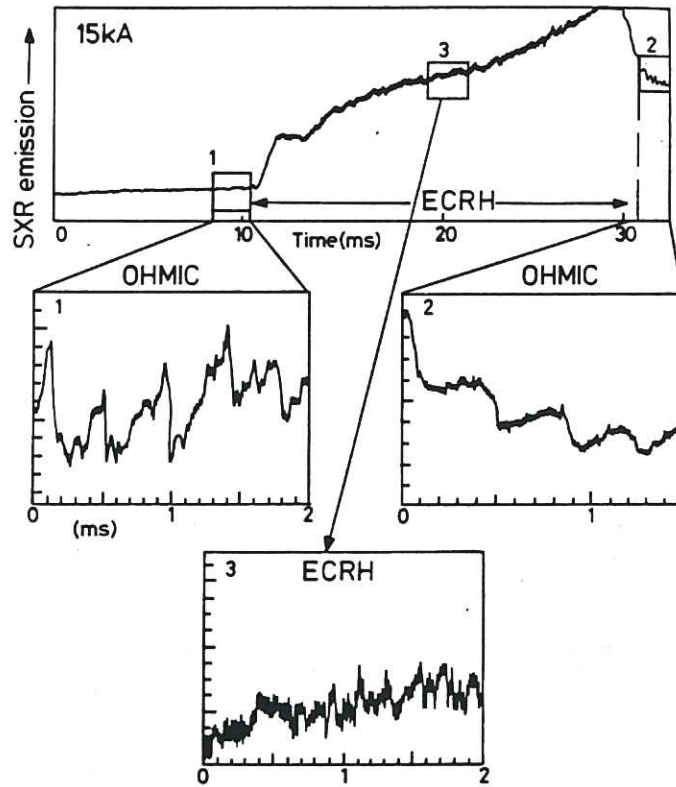
Fig. 7 Line-integrated soft X-ray emission in a 15 kA discharge showing stabilisation of sawteeth during the RF phase.
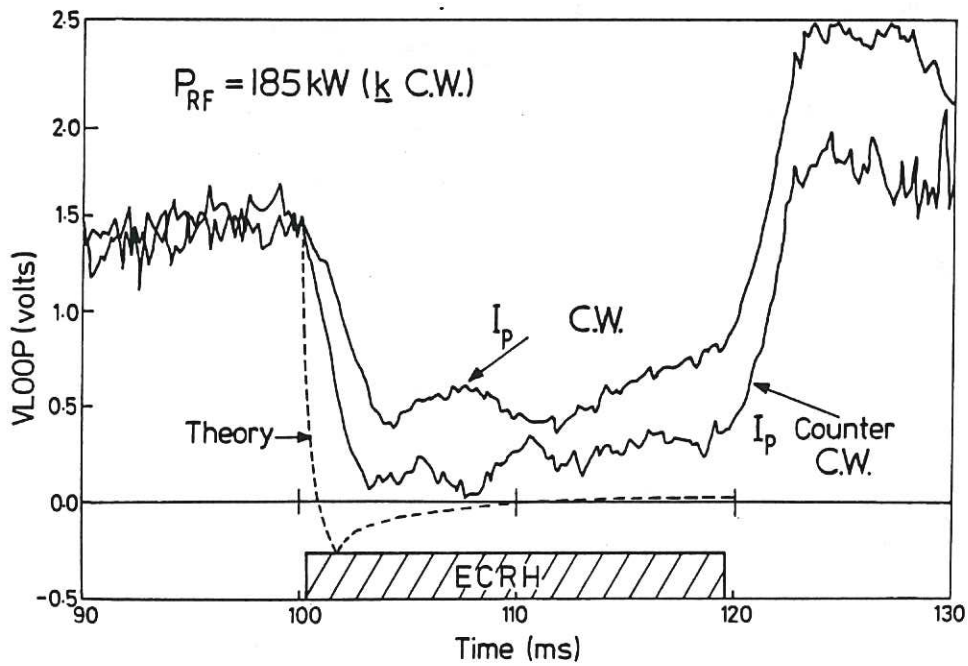
Fig. 8 Time-dependence of loop voltage for CW and CCW plasma current of 10 kA during 60 GHz ECRH. $B_{\phi 0} \sim 1.07$ T and $\bar{n}_e \sim 3.5 \times 10^{18}$ m^{-3}. The dotted curve shows the expected time-dependence for I_p CCW in the presence of a bootstrap current of ~ 7 kA.
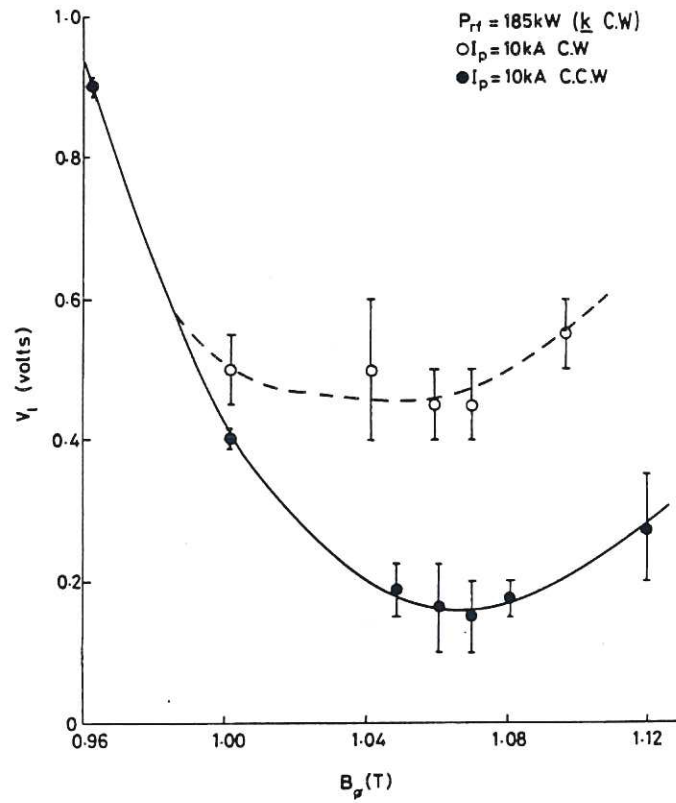
Fig. 9 Loop voltage as a function of central toroidal magnetic field for CW and CCW plasma current of 10 kA during 60 GHz ECRH. The TE_{02} Vlasov antenna is orientated to launch waves with k, CW.
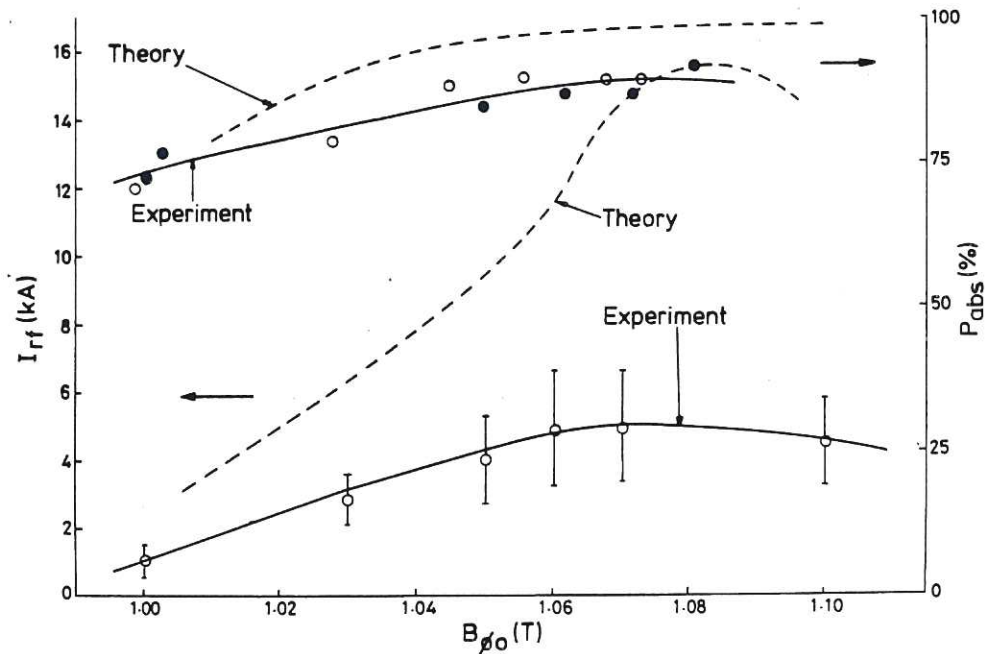
Fig. 10 Comparison of RF driven current as a function of toroidal magnetic field (as deduced from Fig. 9) with theoretical predictions. Also shown are the theoretical and experimental estimates of absorption efficiency where for the latter case the open and closed circles correspond to clockwise and counterclockwise plasma current respectively. $P_{RF} = 185$ kW, $I_p = 10$ kA and $\bar{n}_e \sim 3.5 \times 10^{18}$ m^{-3}.
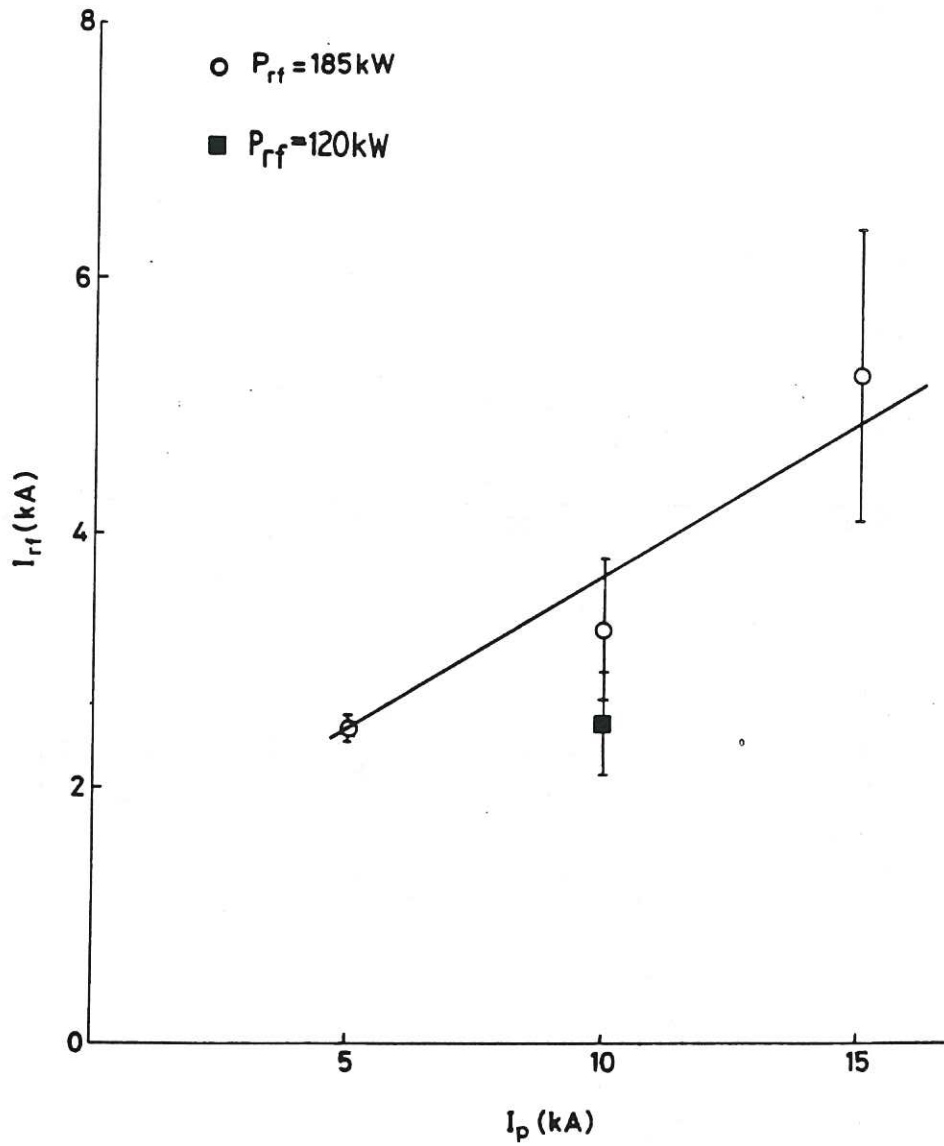
Fig. 11 RF driven current as a function of total plasma current for an injected RF power of 185 kW. Also shown for comparison is the deduced RF driven current for an injected power of 120 kW at $I_p = 10$ kA.
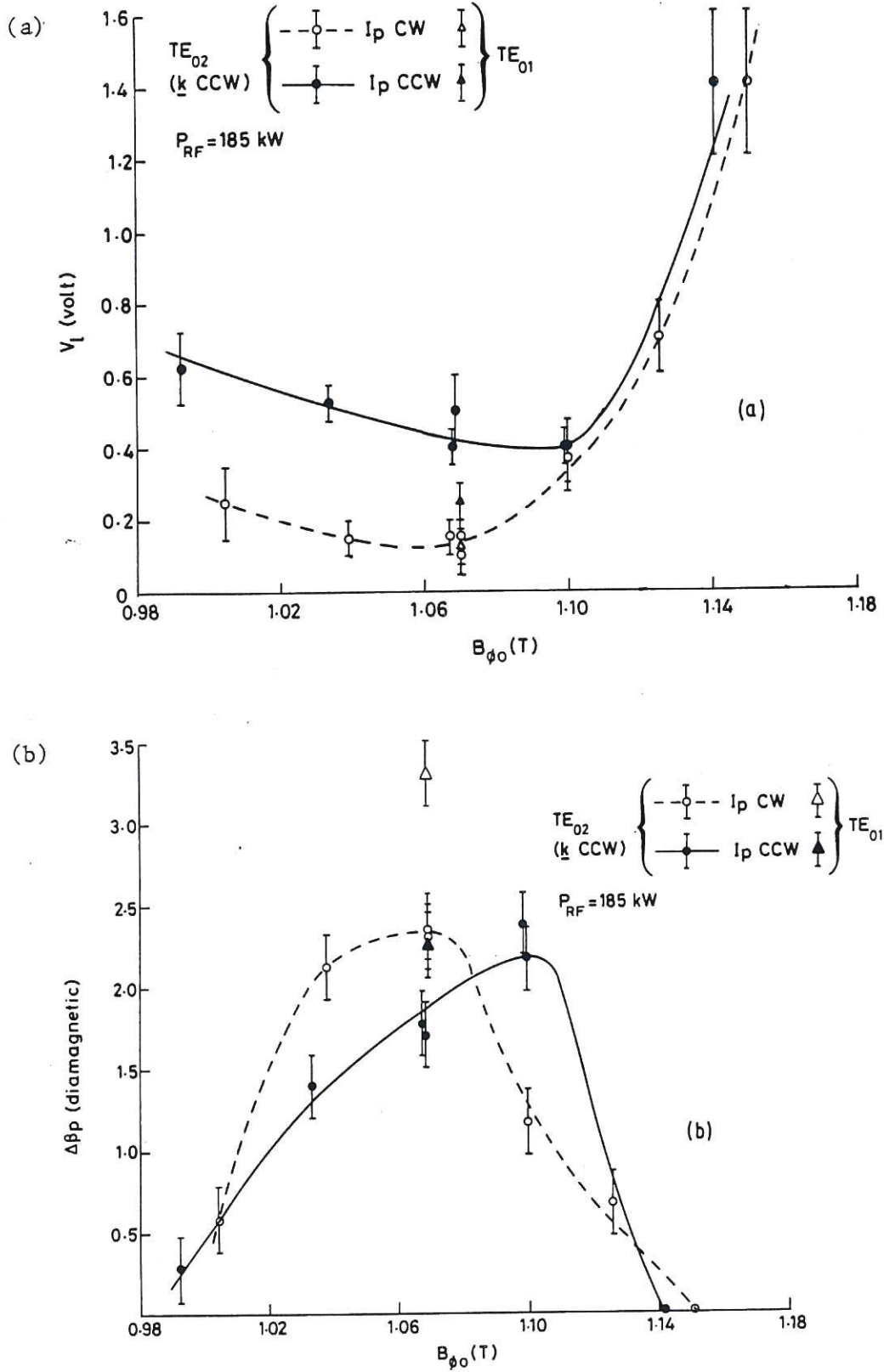
Fig. 12 Toroidal field dependence of (a) loop
voltage and (b) increase in poloidal beta for CW
and CCW plasma current of 10kA during 60GHz
ECRH. The TE_{02} Vlasov antenna is orientated to
launch waves with k CCW. Also shown are points
obtained at $B_{\phi 0} = 1.07$T with the TE_{01} launch
antenna.
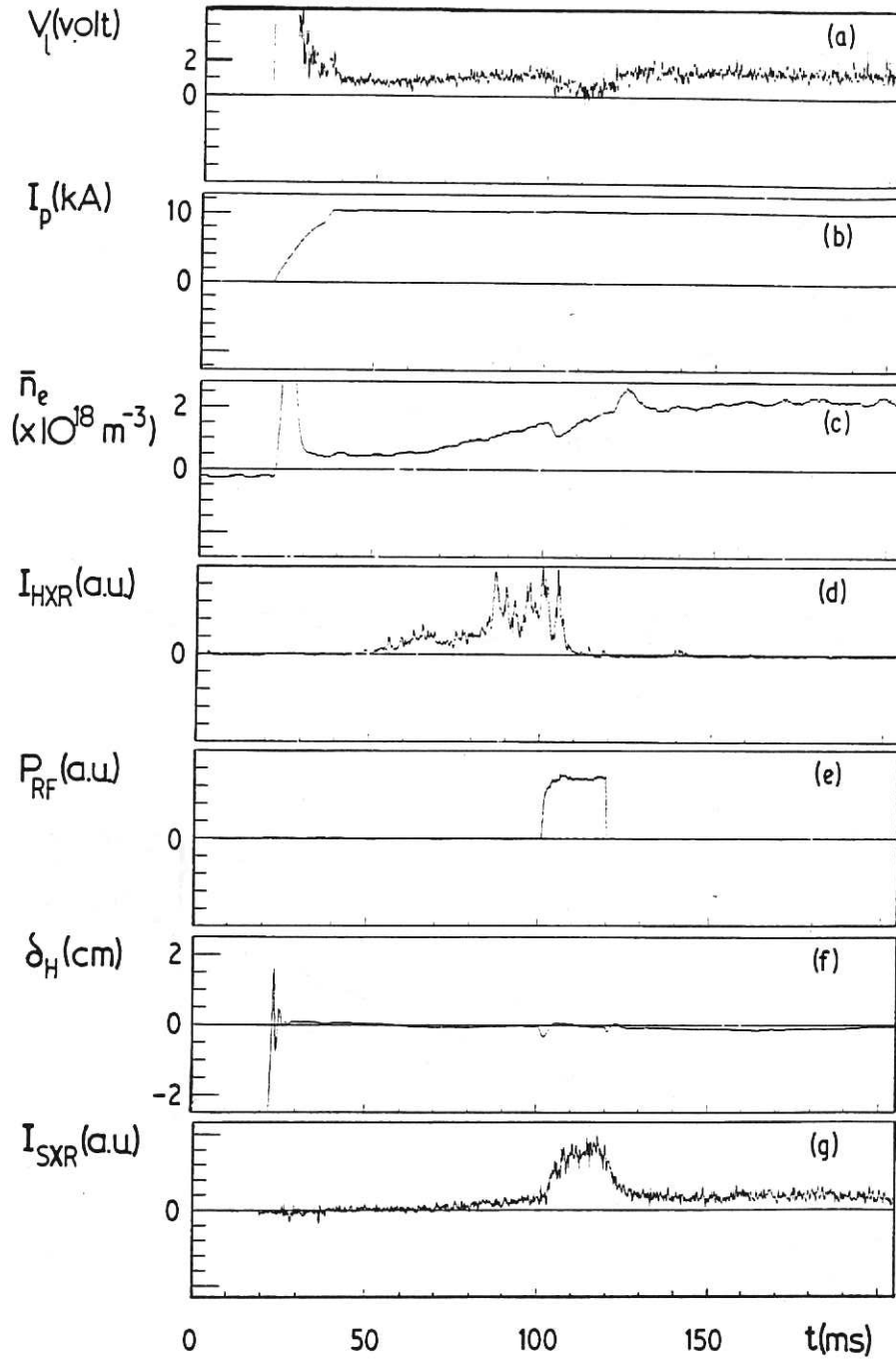
Fig. 13 A typical discharge for 28 GHz current drive studies; $B_{\phi 0} = 0.502\,\text{T}$, $P_{RF} = 120\,\text{kW}$, (a) loop voltage, V_{ℓ}, (b) plasma current, I_p, (c) line-averaged electron density (at $R = R_0$), $\bar{n}_e$, (d) hard X-ray emission, I_{HXR}, (e) RF power, P_{RF}, (f) in-out plasma position, δ_H, (g) line-integrated soft X-ray emission (at $R = R_0$), I_{SXR}.
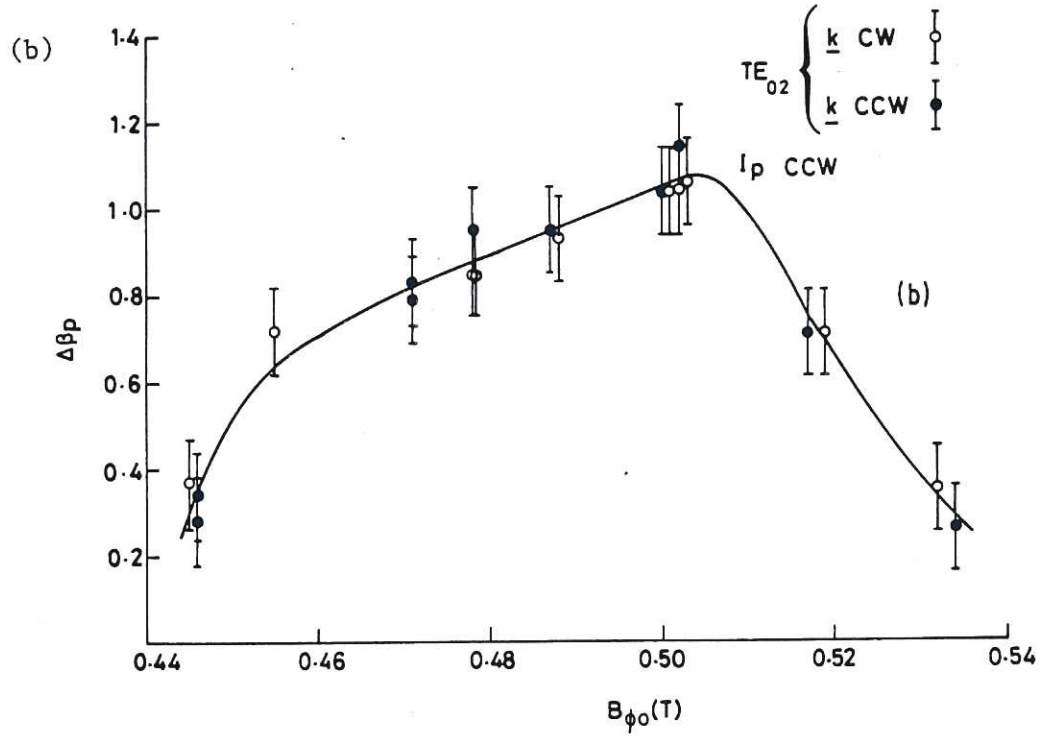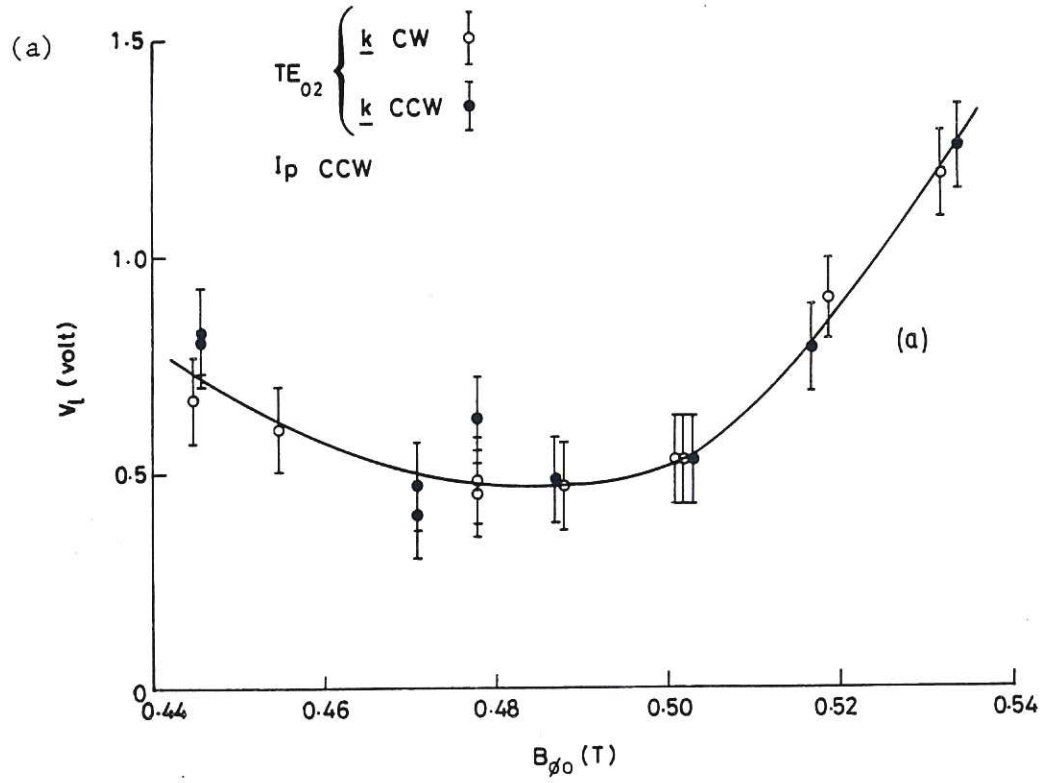
Fig. 14 Toroidal field dependence of (a) loop voltage and (b) increase in poloidal beta for waves launched CW and CCW during 28 GHz ECRH. $I_p = 10$ kA, $P_{RF} = 120$ kW and $\bar{n}_e \sim 2 \times 10^{18}$ m^{-3}.
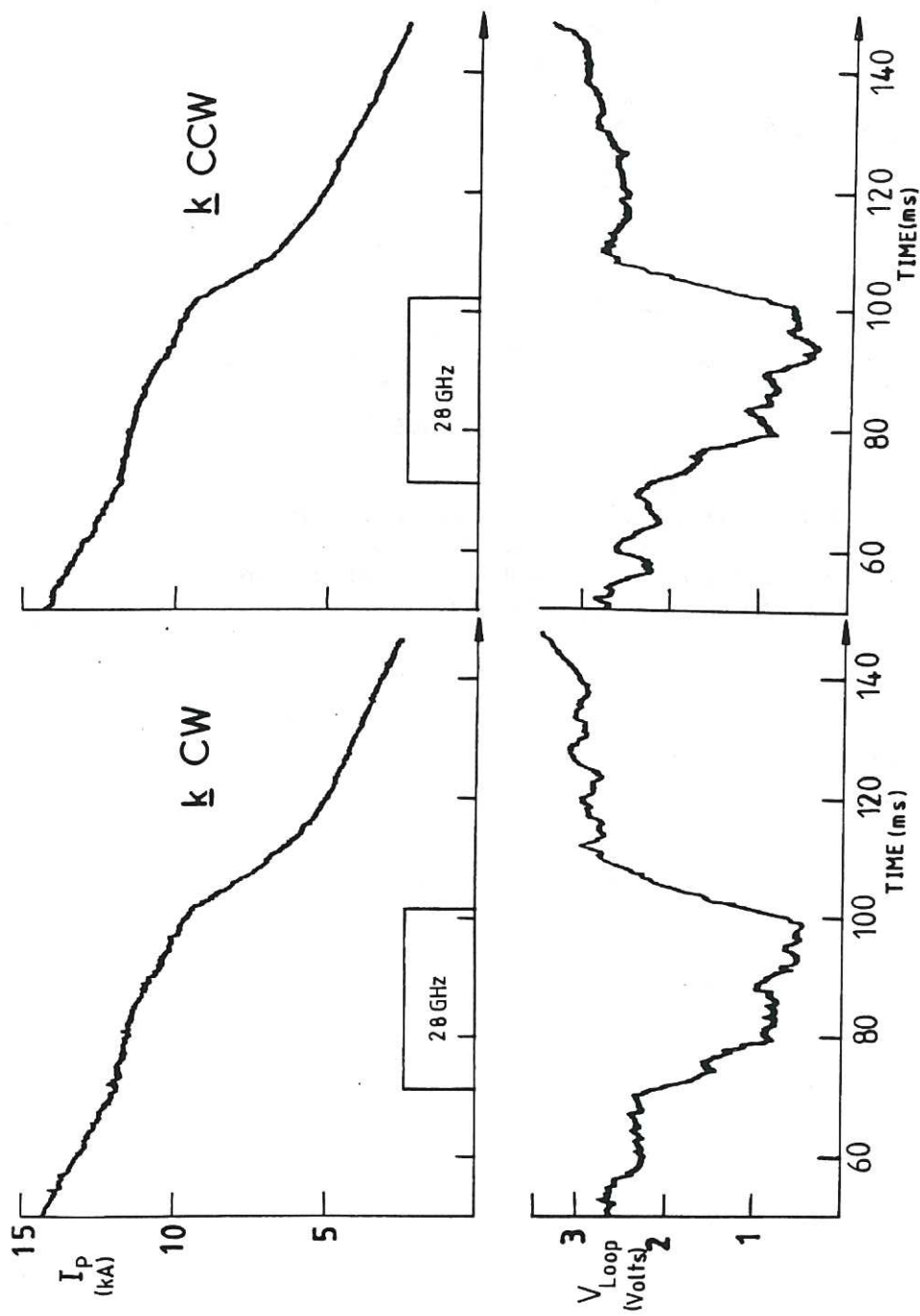
Fig. 15 Time-dependence of plasma current and loop voltage during 28 GHz ECRH for waves launched CW and CCW with the $(TE_{01}+TE_{11})$ antenna. I_p is CW. $P_{RF}=135 kW$ and $\bar{n}_e \sim 2 \times 10^{18} m^{-3}$.
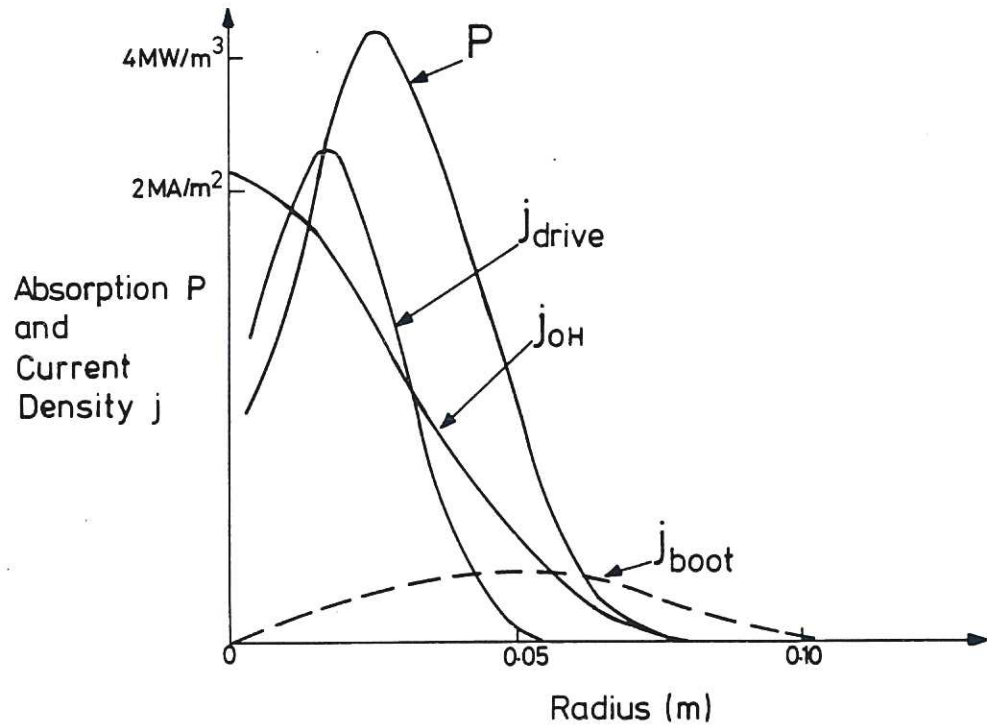
Fig. 16 Predicted profiles of absorbed power P, RF driven
current, inductively driven current j_{OH}, and bootstrap
current, j_{boot}. Displaced circular flux surfaces are
assumed. The abscissa represents the flux surface radius
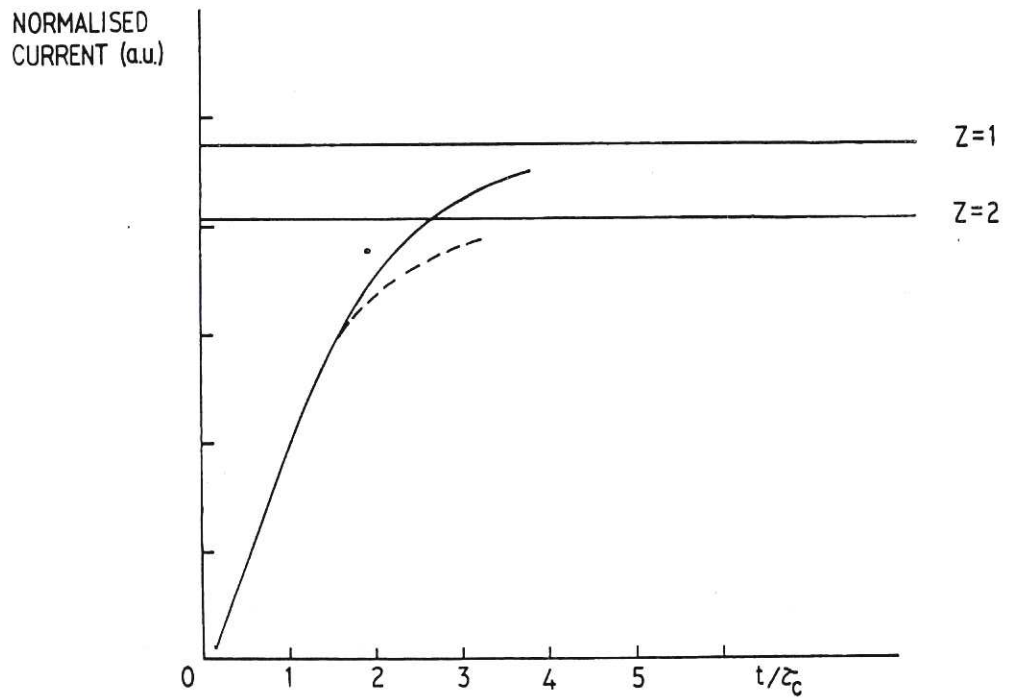so that the magnetic axis is at 0.0m in this representation.

Fig. 17 Evolution of the RF driven current as a function
of time (normalised to the collision time for the resonant
electrons) for $Z_{eff}=1$ and $Z_{eff}=2$.